

Detecting paired and counterflow superfluidity via dipole oscillations

Anzi Hu¹, L. Mathey¹, Eite Tiesinga¹, Ippei Danshita², Carl J. Williams¹ and Charles W. Clark¹

¹Joint Quantum Institute, University of Maryland and National Institute of Standards and Technology, Gaithersburg, MD 20899

² Computational Condensed Matter Laboratory, RIKEN, Wako, Saitama 351-0198, Japan

We suggest an experimentally feasible procedure to observe paired and counterflow superfluidity in ultra-cold atom systems. We study the time evolution of one-dimensional mixtures of bosonic atoms in an optical lattice following an abrupt displacement of an additional weak confining potential. We find that the dynamic responses of the paired superfluid phase for attractive inter-species interactions and the counterflow superfluid phase for repulsive interactions are qualitatively distinct and reflect the quasi long-range order that characterizes these phases. These findings suggest a clear experimental procedure for their detection, and give an intuitive insight into their dynamics.

Rapid progress in experiments with ultra-cold atomic mixtures has made it possible to study the rich quantum many-body phenomena of strongly correlated multi-component systems in a controllable environment [1–7]. In multi-component systems, atoms of different species can form composite particles between different species as a result of inter-species interaction. One well-known example is the Cooper pair in superconductors, formed between spin-up and spin-down electrons as a result of attractive inter-species interaction. The bosonic pairs then condense into a superfluid and flow without dissipation [8]. For repulsive inter-species interactions, particles can bind with holes of other species. Such particle-hole pairing, or anti-pairing, leads to non-dissipative *counter-flow* of the two species while the net flow is zero [9]. In the case of bosonic mixtures, the paired superfluid (PSF) and counterflow superfluid (CFSF) phases compete energetically with the single-particle superfluid (SF) phase. In the strong interaction regime, the ground state can consist of PSF and CFSF phases [10–17].

One intriguing property of a superfluid is dissipationless flow. In experiments of ultra-cold atoms in optical lattices, transport properties are often studied by suddenly displacing a confining harmonic potential and inducing dipole oscillations. This type of experiment has indeed been carried out for investigating the superfluidity of 1D [18, 19] and 3D [20] Bose gases.

In this paper, we report the first many-body simulation to observe counter-flow superfluidity, in a context similar to that originally predicted [9]. We consider the SF, PSF and CFSF states in a 1D binary Bose mixture in an optical lattice confined in a weak harmonic trapping potential [10, 11]. Using the quasi-exact numerical method of time-evolving block decimation (TEBD) [21], we study the transport properties through the dipole oscillations induced by either a brief displacement or a constant displacement of the harmonic trapping potential.

We consider a 1D two-component Bose Hubbard model with a harmonic trap centered at $c_a(t)$,

$$H = \sum_{a=1,2} \sum_j \left\{ -J(b_{a,j+1}^\dagger b_{a,j} + h.c.) + \Omega [j - c_a(t)]^2 n_{a,j} + \frac{U}{2} n_{a,j} (n_{a,j} - 1) \right\} + U_{12} \sum_j n_{1,j} n_{2,j}. \quad (1)$$

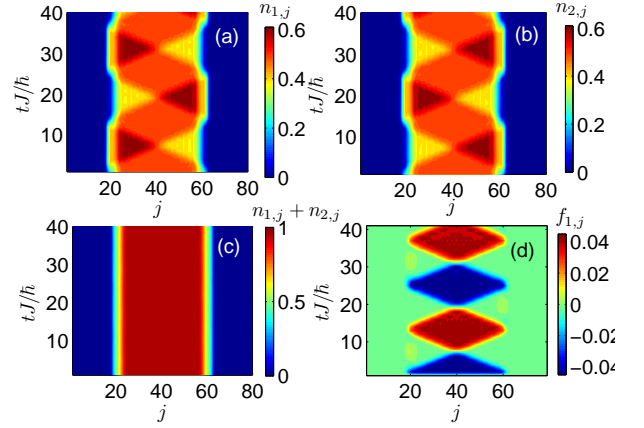


Figure 1: (Color online) Dipole oscillations in the CFSF state after a brief displacement of species 1, where $J/U = 1/14$, $U_{12}/U = 0.6$, $\Omega/U = 10^{-3}$ and time t is in units of \hbar/J . (a), (b): density distributions of species 1 and 2, respectively. At $t = 0$, each species has a plateau at half-filling near the center of the trap. Then, the trap of species 1 is perturbed by a brief displacement as shown in Fig. 2(a). Species 1 and 2 are seen to begin moving in opposite directions, whereas the total density is independent of time as shown in panel (c). (d): local current of species 1, $f_{1,j}$, defined in Eq. (2). A positive current corresponds to motion to the right. The diamond pattern in panel (d) reflects the constant speed of flow.

We denote the atomic species with index a , the lattice site with index j , the number of lattice sites N , the lattice constant d , and we impose hard-wall boundary conditions. In this paper, $N = 80$. The species have the same average filling factor, $\nu = M/N \leq 1$, where M is the number of particles for each species. For all cases reported here, $M = 20$. We also assume that the repulsive intra-species interaction $U > 0$, hopping parameter $J > 0$ and the spring constant Ω are the same for both species. The inter-species interaction is given by U_{12} . The operators $b_{a,j}^\dagger$ and $b_{a,j}$ are the creation and annihilation operators for atoms of type a on site j and $n_{a,j} = b_{a,j}^\dagger b_{a,j}$ is the atom number operator. We assume that the trap centers, $c_a(t)$, are time dependent and independently controllable. Their initial values are $c_a(t = 0) = 40.5$. For convenience, we define the displace-

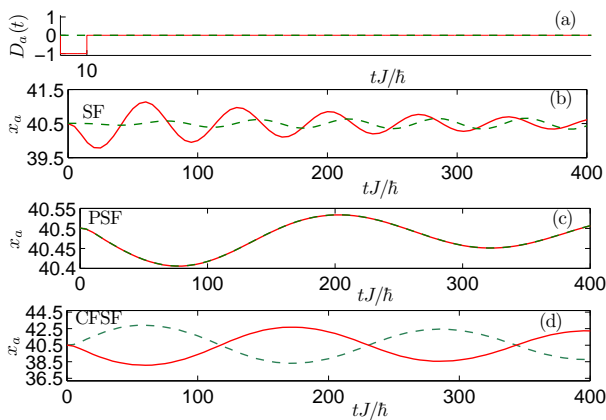


Figure 2: (Color online) Center of mass oscillations of the two species for SF, PSF, and CFSF states induced by a brief trap displacement of species 1. (a): trap displacement vs. time. (b): evolution of the SF state with parameters $J/U = 1/8$, $U_{12}/U = -0.1$, $\Omega/U = 2.5 \times 10^{-4}$. The full (dashed) lines correspond to species 1 (2). (c): PSF state for $J/U = 1/8$, $U_{12}/U = -0.7$, $\Omega/U = 2.5 \times 10^{-5}$. The species oscillate in phase as a result of their pairing order. (d): CFSF state for $J/U = 1/8$, $U_{12}/U = 0.7$ and $\Omega/U = 10^{-3}$. The species oscillate out of phase due to the anti-pairing order.

ment $D_a(t) = c_a(t) - c_a(0)$. The physical effects discussed in this paper can also be achieved by applying magnetic field gradients, which induce linearly varying potentials.

The initial state is the ground state of H at $t = 0$ obtained by the TEBD method with imaginary time propagation. The time evolution is obtained with real-time TEBD propagation with the time step δt equal to $\delta t J/\hbar = 0.05$, where \hbar is the reduced Planck constant. Previous works [22, 23] have applied TEBD to simulate dipole oscillations induced in 1D single-species systems, and successfully explained experimental results [18]. Here, we analyze the time evolution of the system by studying the spatial density distribution $\langle n_{a,j}(t) \rangle$, where the expectation value is over the state of the system, and also the local flux or current

$$f_{a,j} = iJ \langle b_{a,j+1}^\dagger b_{a,j} - b_{a,j}^\dagger b_{a,j+1} \rangle, \quad (2)$$

and the center of mass for each species

$$x_a(t) = \sum_j \frac{j}{M} \langle n_{a,j}(t) \rangle. \quad (3)$$

Additionally we define the center of mass of both species, $x_{\text{total}}(t) = [x_1(t) + x_2(t)]/2$ and the relative center of mass, $x_{\text{relative}}(t) = x_1(t) - x_2(t)$.

We first consider the time evolution after a brief displacement of the harmonic confinement of species 1. Figure 1 shows a compelling example of the *counter-flow* property of the CFSF phase. Particle-hole pairing in the CFSF state requires that the particle density of one species equals the hole density of the other: $\langle n_{j,1} \rangle = \langle 1 - n_{j,2} \rangle$. For equal fillings, this means that the

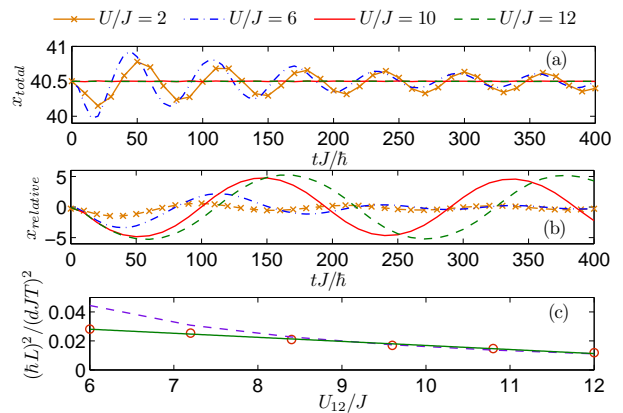


Figure 3: (Color online) Dipole oscillation of the total and relative center of mass; initial displacement as in Fig. 2. (a): $x_{\text{total}}(t)$ for $U/J = 2, 6, 10, 12$; only in the cases of $U/J = 2$ and 6 do we see significant induced oscillation. (b): $x_{\text{relative}}(t)$ for the same U/J . A phase transition from SF to CFSF is induced by changing U/J while keeping U_{12}/U and Ω/U fixed at $U_{12}/U = 0.6$ and $\Omega/U = 10^{-3}$. The transition occurs for $U/J \approx 8$. The transition is reflected in the *sudden* change in the behavior of the center of mass motion. Panel (c) shows the ratio $(\hbar L)^2 / (dJT)^2$ as a function of U_{12}/J in the CFSF region for fixed U_{12}/U , where T is the oscillation period and L is the length of the CFSF plateau extracted from the simulations. The markers are data from our simulations. The full line corresponds to a linear fit and the dashed line corresponds to Eq. (7).

CFSF phase only occurs at half-filling, $\nu = 1/2$ [10]. In a trapped system, the density of the CFSF phase shows a plateau at half-filling near the center of the trap. Near the edges of the trap, the system is in a SF phase. The impulse applied to species 1 is generated by the brief displacement shown in Fig. 2(a). It causes the species to move in opposite directions, as shown in Fig. 1(a) and (b). The density of species a at a given position oscillates about $n_a = 0.5$, and the density oscillations of the two species differ in phase by π . The flux is reflected at the steep SF edge of the atomic cloud. The total density distribution stays unchanged and equals one (see Fig. 1(c)).

Figure 1(d) shows the local current of species 1 as a function of time. At any given time, the flow occurs in only one direction. Moreover, the color image shows characteristic diamond shapes. Within each diamond, the current is nearly independent of lattice site and time, which indicates a constant velocity flow. This constant flow can be understood from the constant total density of the CFSF state. As the energy due to the trapping potential at each site only depends upon the total density there, there is no potential energy cost in changing the local relative density and the observed flow moves freely within the CFSF plateau.

In Fig. 2, we show an example of the center of mass motion, $x_a(t)$, for SF, PSF, and CFSF initial states after applying a small impulse to species 1. For the SF state, Fig. 2(b) shows that only species 1 is excited immedi-

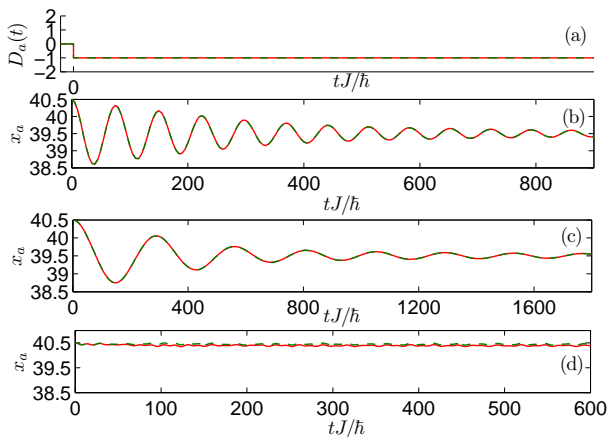


Figure 4: Dipole oscillation of the center of mass of the two species after a sudden displacement. (a): trap displacement vs. time. (b), (c), (d): time evolution for the SF, PSF and CFSF states. The system parameters are the same as in Fig. 2 and the full (dashed) lines correspond to species 1 (2). The depicted time scale differs between panels.

ately after the impulse. Oscillatory motion of species 2 is only induced gradually as a result of the weak attraction between the two species. In Fig. 2(c) we show the response of the PSF phase. Due to the pairing order, both species move instantaneously and the time evolution of the center of mass is identical. The impulse on species 1 is transformed into a collective motion of both species and there is no relative motion. In the CFSF phase shown in Fig. 2(d), we see that the oscillatory motion of species 1 is perfectly matched by an opposite or counter-flowing motion of species 2. We note that the sinusoidal oscillation of the center of mass is not in contradiction with the constant current flow shown in Fig. 1. The averaging over lattice sites as expressed in Eq. (3) has erased this information.

In Fig. 3 we plot the time evolution of the center of mass of both species, $x_{\text{total}}(t)$, and the relative center of mass, $x_{\text{relative}}(t)$, after a brief displacement as in Fig. 2 for several interaction strengths. We increase the intraspecies interaction U from $2J$ to $20J$ and U_{12} from $1.2J$ and $12J$ while we fix the ratio between U_{12} and U at $U_{12}/U = 0.6$ and set $\Omega/U = 10^{-3}$. The system undergoes a phase transition from SF to CFSF around $U/J \approx 8$. In the SF state, the brief displacement of species 1 leads to damped oscillations in both the relative and total center of mass. The maximum amplitude of the oscillation increases with U/J . The damping rate increases in this regime. As U/J increases beyond the critical point, the total center of mass motion is suddenly suppressed to almost zero. On the other hand, the amplitude of the relative center of mass keeps increasing through the phase transition. The damped oscillation of the relative center of mass suddenly changes to nearly undamped above the transition.

We have also studied the dependence of the oscillation

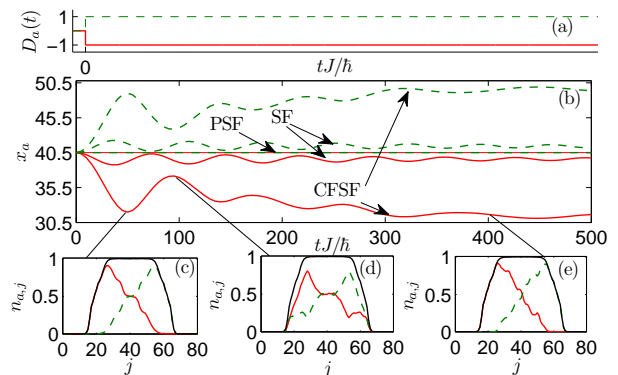


Figure 5: Dipole oscillation of the center of mass after displacing the two traps in opposite directions. (a): trap displacement vs. time. (b): center of mass motion for the SF, PSF and CFSF states. The full (dashed) line corresponds to species 1 (2). (c)-(e): density distributions at $tJ/\hbar = 55, 100$ and 400 , respectively, for the CFSF state. Parameters used for the three states are the same as in Fig. 2.

period on the interaction strength in the CFSF state. As noted previously, the density flow occurs at a constant velocity in this regime. The velocity can be estimated with two methods: the Luttinger liquid theory and an effective spin-1/2 model. The Luttinger liquid theory predicts phonon-like low energy excitations with a phonon velocity

$$v_A \sim \frac{2Jd}{\hbar} \sqrt{1 - AU_{12}/J - BU_{12}/U}, \quad (4)$$

where the non-universal coefficients A and B are assumed to be constants. For a plateau of length L , the period of oscillation is then $T = 2L/v_A$. For the analysis of our simulations, we find it convenient to define the relationship based on Eq. (4),

$$\left(\frac{\hbar L}{dJT} \right)^2 \sim 1 - AU_{12}/J - BU_{12}/U. \quad (5)$$

In the limit of large U_{12}/J and U/J , we can derive another relationship for the period. Assuming the particle-hole pairs are hard-core bosons, Eq. (1) can be mapped to an effective spin-1/2 model [14]. Using linear spin-wave theory[24], we obtain the phonon velocity v_A as

$$v_A = \frac{4J^2d}{U_{12}\hbar} \sqrt{1 - U_{12}/U}, \quad (6)$$

and

$$\left(\frac{\hbar L}{dJT} \right)^2 = 4(J/U_{12})^2(1 - U_{12}/U). \quad (7)$$

Unlike for the Luttinger theory, this relationship does not have free parameters. Figure 3(c) shows the quantity $(\hbar L)^2/(dJT)^2$ as a function of U_{12}/J for fixed U_{12}/U ,

where L and T are obtained from the simulations. Overall, the quantity $(\hbar L)^2/(dJT)^2$ shows a linear trend consistent with the relationship in Eq. (5). The value is in good agreement with Eq. (7) especially for $U_{12}/J > 8.4$.

In Fig. 4 we consider the time evolution after a sudden displacement for the SF, PSF and CFSF initial states. The displacement is the same for both species. For the SF and PSF initial states, the centers of mass of both species oscillate in phase around the new minimum of the trap. The origin of the in-phase motion is different for these two initial states. For the SF state, the species respond independently to the same displacement. For the PSF state, the species respond as pairs. The oscillation frequencies for the SF and PSF states differ. This is not only because the states are confined by different trapping potentials, but also because of the larger effective mass of the pairs in the PSF state. The oscillations exhibit damping that can be attributed to strong quantum fluctuations in 1D systems [18, 22, 23]. For the CFSF state, the motion is overdamped and the center of mass remains at the original equilibrium position. The small oscillations that are visible in the time evolution of $x_1(t)$ and $x_2(t)$ are due to oscillations of the superfluid at the edges of the atomic cloud. For this type of displacement, the impact on both species is the same and it only affects the total density. Because the motion of the total density is suppressed for the CFSF state, the displacement can not induce a response.

In Fig. 5 we consider a sudden displacement of the two traps in opposite directions. For the SF state, the two species oscillate around their respective new trap minima. The PSF state has no response, because the pairing order resists the force imparted by the trap displacement. The most dramatic response is in the CFSF state. Because the displaced traps act as an effective linear potential,

$2\Omega(D_1 + D_2)j$, on the relative density, the two species are driven to move apart, until they reach the edge of the CFSF plateau. 5(c)-(e) show density profiles at different times during the time-evolution.

By increasing the displacement amplitude, we can potentially break the (anti-)pairing order. We can break the PSF pairing by applying a large opposite displacement, while the CFSF pairing can be broken by a large identical displacement. The displacement amplitude then becomes an indicator of the binding energy of the pairs in the PSF state and the anti-pairs in the CFSF state.

In conclusion, we have studied the dipole oscillation of 1D two-component Bose mixtures in an optical lattice and a weak confining harmonic potential. The oscillation is induced by displacing the harmonic confinement either briefly or suddenly. We have shown that the response of the system shows much richer features than its single-component counterpart. In the two-component system, there are three long-range orders: the superfluid, paired superfluid and counter-flow superfluid orders. For the PSF and CFSF states, the suppression of individuality leads to distinct dipole oscillations dependent on the character of the perturbation. We have shown that this is the consequence of pairing and anti-pairing ordering for the two states. For the CFSF state, which forms plateaus of constant total density, the dipole oscillations resemble the oscillation of a confined homogeneous system with free propagation between boundaries.

We acknowledge helpful discussions with Trey Porto, Steven Olmschenk, Dominik Schneble and Yoshiro Takahashi. This work was supported by the U. S. Army Research Office under the Atomtronics MURI Program. I.D. is supported by KAKENHI (22840051) from JSPS. The computational work reported here was partially done on the RIKEN Cluster of Clusters facility.

-
- [1] J. Catani, *et al.*, Phys. Rev. A **77**, 011603 (2008).
 - [2] B. Gadway, *et al.*, Phys. Rev. Lett. **105**, 045303 (2010).
 - [3] A. Widera, *et al.*, Phys. Rev. Lett. **100**, 140401 (2008).
 - [4] S. Ospelkaus, *et al.*, Phys. Rev. Lett. **96**, 180403 (2006).
 - [5] K. Günter, *et al.*, Phys. Rev. Lett. **96**, 180402 (2006).
 - [6] T. Best, *et al.*, Phys. Rev. Lett. **102**, 030408 (2009).
 - [7] C. A. Regal, *et al.*, Phys. Rev. Lett. **92**, 040403 (2004)
 - [8] L.N. Cooper, Phys. Rev. **104** 1189 (1956); J. Bardeen, *et al.*, Phys. Rev. **106** 162 (1957); Phys. Rev. **108** 1175 (1957).
 - [9] A. B. Kuklov and B. V. Svistunov, Phys. Rev. Lett. **90**, 100401 (2003).
 - [10] A. Hu, *et al.*, Phys. Rev. A **80**, 023619 (2009); A. Hu, *et al.*, Phys. Rev. A **81**, 063602 (2010).
 - [11] L. Mathey, *et al.*, Phys. Rev. A **79**, 013609 (2009).
 - [12] B. Paredes and J. I. Cirac, Phys. Rev. Lett. **90**, 150402 (2003).
 - [13] A. B. Kuklov, *et al.*, Phys. Rev. Lett. **92**, 030403 (2004); *ibid.* Phys. Rev. Lett. **92**, 050402 (2004); Phys. Rev. A **69**, 025601 (2004).
 - [14] E. Altman, *et al.*, New J. Phys. **5**, 113 (2003).
 - [15] Ş.G. Söyler, *et al.*, New J. Phys. **11**, 073036 (2009).
 - [16] T. Ohgoe and N. Kawashima, Phys. Rev. A **83**, 023622 (2011).
 - [17] C. Trefzger, *et al.*, Phys. Rev. Lett. **103**, 035304 (2009); C. Trefzger, *et al.*, New J. Phys. **12** 093008 (2010).
 - [18] C. D. Fertig, *et al.*, Phys. Rev. Lett. **94**, 120403 (2005).
 - [19] T. Stöferle *et al.*, Phys. Rev. Lett. **92**, 130403 (2004); E. Haller *et al.*, Nature **466**, 597 (2010).
 - [20] S. Burger *et al.*, Phys. Rev. Lett. **86**, 4447 (2001).
 - [21] G. Vidal, Phys. Rev. Lett **91**, 147902 (2003); *ibid.* **93**, 040502 (2004); S. R. White, *et al.*, Phys. Rev. Lett. **93**, 076401 (2004);
 - [22] I. Danshita and C. W. Clark, Phys. Rev. Lett. **102**, 030407 (2009).
 - [23] S. Montangero, *et al.*, Phys. Rev. A **79**, 041602(R) (2009).
 - [24] See, e.g., R. M. White, *Quantum Theory of Magnetism* (Springer, New York, 2006).